10,03

The dynamics of screening of an external electric field in potential walls of the InGaN/GaN quantum well

© N.I. Bochkareva, Yu.G. Shreter¶

Ioffe Institute,
St. Petersburg, Russia

¶ E-mail: y.shreter@mail.ioffe.ru

Received November 9, 2023
Revised November 9, 2023
Accepted February 4, 2024

The dynamics of external electric field screening in light-emitting $p-n$ heterostructures with InGaN/GaN quantum wells are studied using measurements of transient currents during a forward voltage step and small-signal high-frequency conductance at a direct forward voltage. Experimental results are discussed within the framework of a model that takes into account the increase in tunneling transparency of potential walls of a quantum well by a strong built-in field, which is created by ionized deep centers of defects. At low levels of tunneling injection, the tunneling transparency of the walls increases as the forward bias increases due to an increase in the density of ionized states at the hole tunneling transport level, which leads to an increase in the emission efficiency from the quantum well. The recharging of deep centers and the accumulation of neutral centers is manifested in the capacitive decay of transient current. As the injection level increases, the emission efficiency begins to decrease as a result of an exponential increase in the number of recombination centers and a decrease in the lifetime in the well walls, causing an inductive rise of tunnel-recombination current in the walls and the appearance of negative capacitance.

Keywords: gallium nitride, quantum well, tunneling, quantum efficiency, negative capacitance.

DOI: 10.61011/PSS.2024.03.57946.250

1. Introduction

The dynamics of screening of an electrical field in semiconductor materials with deep centers determines operation of electronic devices with barrier structures and is widely used to determine parameters of the deep centers.

In the GaN epitaxial layers and the InGaN/GaN quantum wells, the localized states of the deep centers form deep Urbach tails that exponentially fall deeply inside a band gap [1–3]. The unordered semiconductors and the structurally-disordered quantum wells have energy relaxation of the optically injected carriers progressed in two stages: fast direct capturing of photocarriers to the localized states of the exponential Urbach tail is accompanied by slow redistribution of the captured carriers between the local centers [4–6]. Diffusion in the energy space occurs as a result of tunnel jumps of the photocarriers from the shallow localized states into the deeper states [4–6]. When tunneling the electrically injected carriers through a potential barrier, the carriers diffuse in the coordinate space by tunnel jumps from the shallow local centers into the deeper centers, whose low concentration limits the tunnel current. In this case, as can be expected, the dynamics of setting of the stationary current must also be of a two-stage nature, which is defined by a short Maxwell time and an exponentially slowing time of a jump transition through the barrier.

With the doping degree increased and under radiation effects, the deep centers of the defects, in addition to the Urbach tails, form wide peaks of the density of the deep states in the band gap of the semiconductors and result in strong increase of tunnel transparency of the potential barriers, as originally shown by Esaki [7,8] and confirmed in other early studies [9–11]. In the GaN epitaxial layers, the growth defects, in addition to the deep Urbach tails, create, in the upper and lower halves of the band gap, the wide (~ 0.4 eV) Gaussian impurity bands of the deep color centers that are responsible for bands of intracenter photoluminescence and optical absorption in the visible, infrared and near UV ranges of the spectrum [12–15]. The recent decade has seen a grown interest to the tunneling mechanism with involvement of the deep centers. It is related to a necessity of understanding a cause of and minimizing trap-assisted tunneling losses (TAT) in the field transistors [16] and light-emitting diodes based on GaN [17], and is also caused by developing the 3D and 2D tunnel field transistors [18,19] and multi-transition solar cells [20]. Both the recent theoretical studies [21–23] and the early studies [8,9] regard current-voltage curves of the tunnel structures in the direct biases as tunnel spectra of the density of the localized stated in the band gap. The studies [24–26] have paid attention to the fact that if the width of the energy impurity bands exceeds thermal energy, then it is critically important to increase the tunnel transparency of the barrier by means of the bulk charge of the ionized deep centers that increase the strength of the built-in electric field. At the same time, a current-voltage curve shape and a structure efficiency

begin to be decisively affected by reduction of the tunnel transparency caused by recharging of the deep centers as the forward bias increases. The dynamics of screening of the external field in the barrier structures will let more deeply understand the tunneling mechanism with involvement of the deep centers and the role of the defects in these structures.

The present study investigates peculiarities of the dynamics of screening of the electric field and setting of the stationary forward current in the light-emitting $p-n$-heterostructures with the InGaN/GaN quantum wells by means of measuring the transient currents at pulse switching-on of forward voltage and small-signal high-frequency conductance at the direct voltage in order to more deeply understand the mechanism of transport in these structures and its influence on confinement of the charge carriers and efficiency of emission from the quantum well.

2. Experimental procedure

The studies have been performed in the light-emitting heterostructures with the p-GaN/InGaN/n-GaN quantum well of the thickness of 30 Å and the peak emission energy of $h\nu_p = 2.65\,\text{eV}$ (the structure area $S = 10^{-3}\,\text{cm}^2$). It included investigation of MOCVD-grown structures of the two types (hereinafter referred to as A and B) that have close values of the tunnel leak currents near the zero voltage and differ in 3 orders when the forward voltage approaches the threshold voltage of detection of emission from the quantum well $V_{th} = 2.2\,\text{V}$. In accordance with the measurements of the capacitance-voltage curves, the A nanostructures with high leak currents have the p-region more weakly doped ($\sim 2 \cdot 10^{17}\,\text{cm}^{-3}$) than the n-region ($10^{18}\,\text{cm}^{-3}$), and the B nanostructures with low leak currents have the p- and n-regions strongly doped ($> 3 \cdot 10^{18}\,\text{cm}^{-3}$). The structure details are shown in [27,28].

The transient currents of the structures were measured in application of rectangular pulses of forward voltage of the amplitude $V_p = 0.3-3.2\,\text{V}$, the duration $t_p = 1-100\,\mu\text{s}$ and the repetition rate $f = 1\,\text{kHz}$. The value of the initial current I_{p0} was limited by the total resistance $R_s = R_L + R_l$ of the structure-serial limiting resistance $R_L = 1\,\text{k}\Omega$ and load resistance $R_l = 100\,\Omega$. The voltage at the load resistance in proportion to the transient current was analyzed by a boxcarintegrator BCI-280. The transient currents were measured by gating the voltage pulses on the load resistance within the time interval $10\,\text{ns}-30\,\mu\text{s}$ at the various time shifts of the gating pulse Δt from the pulse front and the gate time $10-400\,\text{ns}$ with accumulation of the n-th ($n = 8-128$) number of the pulses in order to improve the signal-to-noise ratio. The time dependences of transient current $I_p(t)$ were used to construct the series of the dependences of instant values of the transient current at the fixed time shift Δt from the voltage pulse amplitude $I_p(V_p)$ for the various Δt within the interval $\Delta t = 50\,\text{ns}-10\,\mu\text{s}$.

The static current-voltage curves were measured by means of Keithley 238. The reactive and active components of small-signal admittance were measured at the frequency of 1 MHz by means of the CV analyzer Keithley 590 with parallel substitution arrangement. The small-signal admittance was measured by applying direct forward voltage and small high-frequency voltage to the $p-n$-structures. The intensity of emission and the external quantum efficiency were measured using an integrating sphere and a calibrated Si-photodiode.

3. Experimental results and discussion thereof

3.1. Manifestation of the Gaussian impurity bands in GaN in the stationary and transient tunnel-recombination current of the nanostructure

The typical dependences of stationary current $I(V)$ on voltage applied in a straight direction are shown on the Figures 1 and 2 (the curves *1*) for the two A nanostructures and on Figure 2 (the curve *2*) for the B nanostructure. The light-emitting structures with the InGaN/GaN quantum well are typically characterized by appearance of the static $\lg I-V$-characteristics of the A nanostructures with the current „shoulder" of tunnel leak within the subthreshold voltages $V < V_{th} = 2.2\,\text{V}$ and with fast current rise at $V > V_{th}$ already slowing at the small currents $I \approx 1\,\text{mA}$ (when current limitation is still neglected by the serial resistance of the structure r_s, which is equal to the sum of the current spreading resistances in the GaN layers and the contact resistances (when $S = 10^{-3}\,\text{cm}^2$ r_s is about $10\,\Omega$).

The nitride $p-n$-nanoheterostructures are asymmetric: the biggest part of contact potential falls into the p-regions due to a high effective mass of holes as well as to a smaller degree of doping of the p-GaN layers than the n-GaN layers. In the direct biases, the tunnel current in the structure is limited by the tunnel resistance of the p-barrier, which, in turn, is determined by tunnel transparency of the potential wall of the quantum well in the p-barrier.

The tunnel current is proportional to a product of the density of the occupied initial states $\rho_s(E_t)$, probability of tunneling through the wall $D(E_{tp})$ (the tunnel transparency of the wall) and the total density of the empty finite states of the impurity band $\rho_{Gf}(E_{tp})$ and the Urbach tail $\rho_{Uf}(E_{tp})$ at a hole tunnel transport level E_{tp}, which passe horizontally in the well wall w_{QW} (Figure 3) [8,9]:

$$I(E_{tp}) \propto \rho_s(E_{tp})\Big(D(E_{tp})\big(\rho_{Gf}(E_{tp}) + \rho_{Uf}(E_{tp})\big)\Big).$$

The probability of tunneling through a triangular potential barrier exponentially depends on the barrier height V_b and the tunneling length $\delta = Vb/qF_b$ (the barrier

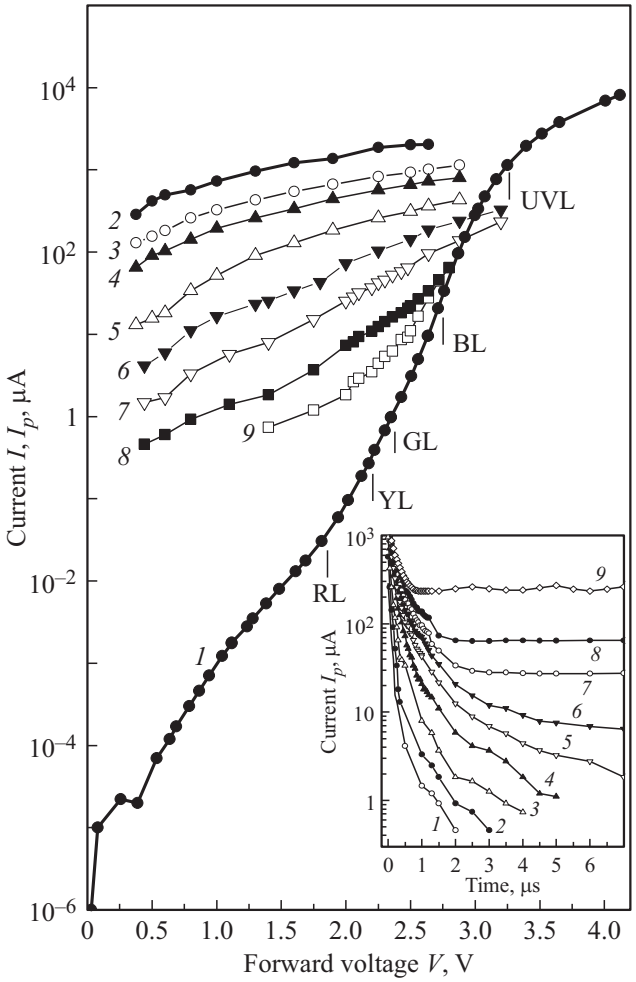

Figure 1. Dependences of stationary forward current $I(V)$ on direct voltage (*1*) and transient forward current $I_p(V_p)$ on the amplitude of the voltage pulse of duration of $t_p = 100\,\mu$s (*2*–*9*) of the A structure. The time shift of the gating pulse Δt, μs: *2* — 0.0, *3* — 0.05, *4* — 0.1, *5* — 0.25, *6* — 0.5, *7* — 1, *8* — 2, *9* — 5. The markers indicate the voltage corresponding to the peak energies of the photoluminescence bands of RL-, YL-, GL-, BL- and UVL-centers in GaN. The inset has the time dependences of the transient current for the A structure. V_p, V: *1* — 0.4, *2* — 0.8, *3* — 1.3, *4* — 2, *5* — 2.25, *6* — 2.5, *7* — 2.64, *8* — 2.9, *9* — 3.2.

width), $Fb = (qN^- V_b/\varepsilon_0\varepsilon)^{1/2}$ — the strength of the electric field [29]:

$$D(E_t) = \exp\left(-\frac{\pi}{2\sqrt{2}\hbar}\,\delta\sqrt{2m^* V_b}\right).$$

Here, q — the electron charge, ε_0 — the electric constant, ε — the dielectric constant, m^* — the effective mass, $N^- = N_a + N_U^- + N_G^-$ — the total concentration of the main dopant — the acceptors N_a, the ionized deep centers of the Urbach tail N_U^- and the Gaussian impurity bands $N_G^- = \sum_i N_{Gi}^-$.

The ionized deep centers increase the strength of the electric field in the space charge region w (SCR) of the barrier of the height of E_0 and its tunnel transparency, thereby reducing the injection barrier in direct voltages and allowing the holes tunneling into the quantum well through the potential wall w_{QW} through the effective barrier of the height of E_{eff} (Figure 3). The holes are thermalized into the localized stats of the Urbach tail of the quantum well. Due to a condition of neutrality preservation, a required number of electrons are tunneled from the *n*-region into the quantum well and in thermalizing, recombine in pairs: radiatively with the localized holes in the Urbach tail of the well and nonradiatively with the localized holes in the wall of the well w_{QW}. As the direct voltage rises, due to recharging of the deep centers and reduction of the bulk charge in the wall w_{QW}, the tunnel transparency of the wall

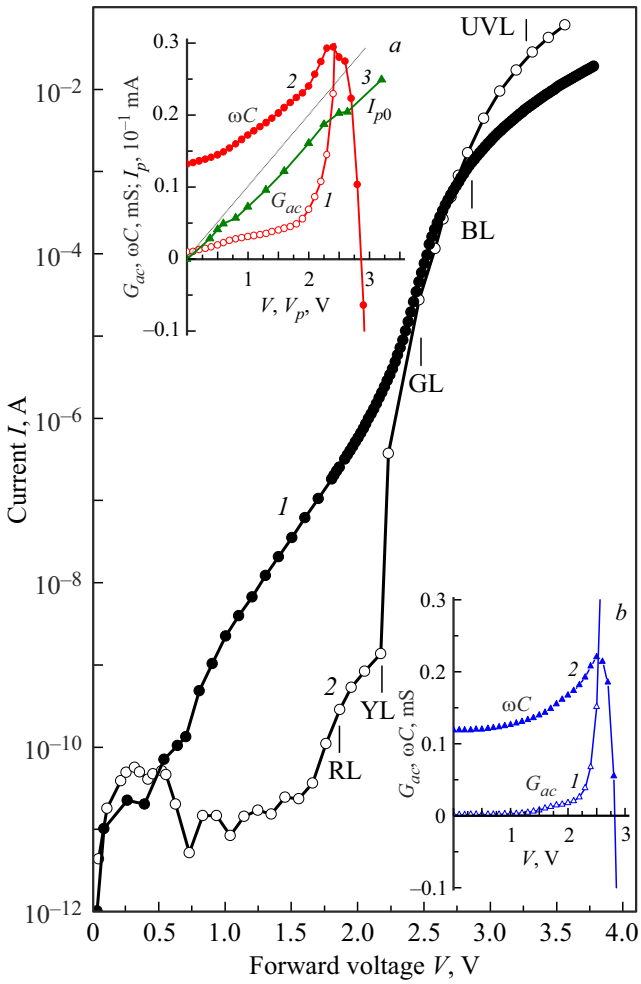

Figure 2. Dependences of forward current on direct voltage for the A (*1*) and B (*2*) structures. The markers indicate the voltage corresponding to the peak energies of the photoluminescence bands of RL-, YL-, GL-, BL- and UVL-centers in GaN. The insets include the dependences of the small-signal amplitudes of active G_{ac} (*1*) and capacitance reactive ωC (*2*) components of the small-signal admittance at the frequency of 1 MHz for the A (*a*) and B (*b*) structures and the dependence of the initial transient current (*3*) for the A (*a*) structure on the voltage pulse amplitude. The dashed line marks the dependence of the maximum possible initial current on the pulse amplitude.

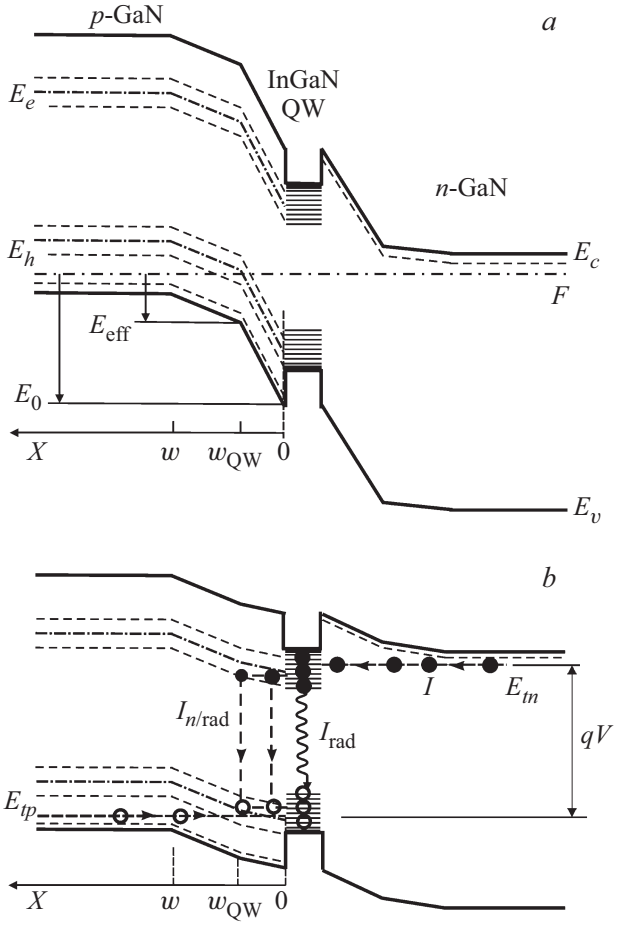

Figure 3. Schematic energy diagram of the light-emitting structure with the *p*-GaN/InGaN/*n*-GaN quantum well in thermal equilibrium (*a*) and in forward bias (*b*), which illustrates increase in the tunnel transparency of the quantum well walls by the ionized color deep centers (*a*), as compensated in direct bias (*b*).

decreases to compensate an increment of the tunnel current caused by barrier reduction.

A fine structure of the current-voltage curve of the B nanostructure (Figure 2, the curve *2*) indicates presence of several impurity bands of the deep centers. The peak of the tunnel current at the small voltages is caused by the Gaussian impurity band $N_{Gi}(E)$, $i = 1$ in the wall of the quantum well and sharp rise of the density of the empty finite ionized states of the band for the holes (tunneling along the tunnel transport level E_{tp}) with increase in the voltage and movement of the level E_{tp} towards the valence band ceiling in the region $E_{tp} < E_{ih}$ (E_{ih} — the energy position of the Gaussian's maximum). The subsequent sharp decrease in the current with increase in the voltage within the region $E_{tp} < E_{ih}$ is caused by recharging of the band states and accumulation of the band neutral states, thereby reducing the bulk charge and the electric field in the well wall, causing reduction of the tunnel transparency of the wall and suppressing the contribution of the shallower Gaussian impurity bands and the Urbach tail to the tunnel conductivity up to $V = 1.65$ V. A stepwise rise of the current in the B structure at $V > 1.65$ V can be related to tunnel transport level Etp's intersection of the impurity bands of the RL-, YL-, GL-, BL- and UVL-centers [24,25] that are responsible for red, yellow, green, blue and ultraviolet photoluminescence in GaN [12–15]. The A structure (the Figures 1 and 2, the curves *1*), where relative contribution of the Urbach tail's states to the total density of the localized states is great, the recharging of the states of the deep Gaussian bands does not result in appearance of negative differential resistance and causes only steps on the curves $\lg I(V)$ within the region $0 < V < 1$ V.

The inset of Figure 1 (the curves *1*–*9*) shows the time dependences of the value of the transient current $I_p(t)$ after the front of the rectangular voltage pulses of duration of $t_p = 100\,\mu$s, as measured at the various pulse amplitudes within the interval $V_p = 0.375$–3.2 V, for the A structure, whose CVC is shown on Figure 1, the curve *1*. As can be seen on Figure 1 and the inset thereof, the initial transient current measured at the front of the voltage pulse of the small amplitude $V_p = 0.4$–0.8 V, exceeds the stationary current by more than seven orders. The transient current drops most rapidly at small voltage surges $V_p = 0.4$ V (the curve *1*), being still higher than the stationary current by 4 orders at $t_p = 10\,\mu$s. With the high voltage surges $V_p = 3.2$ V (the curve *9*), the transient current drops most slowly, but at $t_p = 10\,\mu$s it is in several times less than the stationary current. The exponentially-timed drop of the transient current does not obey the stretched-exponent law $I_p \sim \exp(-(t/\tau_p)^\beta)$ with a characteristic time τ_p and an stretching exponent of the exponential function $\beta < 1$ (both are constant for the time of relaxation), which is used to describe the relaxation processes in unordered materials. The curves $I_p(t)$ have portions, at which the exponential drop is accelerated and then decelerated forming a step on the curve $I_p(t)$, and it is accelerated again thereafter. With the pulse amplitudes $V_p > 2.5$ V (the curves *6*–*9*) and at $t > 2\,\mu$s the steps of the curves $I_p(t)$ become weak (the curve *6*), and with increase in V_p, instead of a shelf, the curves $I_p(t)$ exhibit a weak increase in the transient current, which is distinct on the curves $I_p(t)$ in a linear scale. The noted peculiarities of the dynamics of the transient current are caused by the ionized states of the Urbach tails and the impurity bands of the color centers with the localization energies $E_{loc} < F$ at the zero forward voltage ($V_p = 0$ V) that are available in the *p*-barrier and by their subsequent recharging when capturing the tunneling holes after surge of the forward voltage V_p during setting the stationary tunnel-recombination current, when the deep centers with the localization energies $E_{loc} > qV_p$ become neutral.

Figure 1 (the curves *2*–*9*) also shows the dependences of the initial transient current $I_{p0}(V_p)$ (the curve *2*) and the instant values of the transient current $I_p(V_p)$ (measured at the various gate time shifts Δt from 50 ns to 5 μs (the curves *3*–*9*) on the pulse amplitude within the interval $V_p = 0.375$–3.2 V for the A structure, which are obtained from the time dependences of the transient current $I_p(t)$.

The initial transient current is below the value of the maximum possible initial current I_m specified by the limiting resistance R_s, as shown by comparing the dependence $I_{p0}(V_p)$ of the inset of Figure 2, the curve *3* and the linear dependence $I_m(V_p) = V_p/R_s$ shown by the dashed line. Besides, the dependence $I_{p0}(V_p)$ has distinct steps near $V_p = 0.5$ and 2.2 V, which correspond in magnitude to the direct voltages $V = 0.5$ and 2.2 V, at which there is evidently sharp increase in the stationary current in the A and B structures (Figure 2, the curves *1* and *2*). The dependences $I_p(V_p)$ (Figure 1, the curves *3*–*9*) also show distinct steps near the voltages $V_p = 0.5$ and 2.2 V, as well as near $V_p = 1.65$ V that corresponds to the direct voltage $V = 1.65$ V, at which there is evidently sharp increase in the direct current in the B structure (Figure 2, the curve *2*).

3.2. Correlation of step rise of the components of small-signal conductivity and transient and stationary current in direct bias

The small-signal conductivity has been measured at the frequency of $f = 1$ MHz to show that in addition to the expected capacitance reactive conductance the p–n-structures exhibited a active conductance component that is comparable in amplitude with the capacitance component within the voltage region $V < 2.8$ V, and an inductive reactive conductance component within the voltage region $V > 2.8$ V. The dependences of the small-signal amplitudes of the active G_{ac} and reactive ωC components of the high-frequency admittance at the frequency of $f = 1$ MHz on the forward bias for the A and B structures are shown on the insets of Figure 2 (the curves *1* and *2*) (here, C — the capacitance being measured, $\omega = 2\pi f$ — the angular frequency).

In the A structure (the inset above), the curves $G_{ac}(V)$ (the curve *1*) exhibit the stepped increase in the amplitude of the active conductance component G_{ac} near the same voltages $V = 0.5$ and 2.2 V, at which there is also evidently a fast rise of the stationary current (Figure 2, the curve *1*), and corresponding to the amplitudes V_p, at which there is evidently a fast rise of the transient current at the time shift $\Delta t = 0.5\,\mu$s (Figure 1, the curve *6*), which is in magnitude close to a high-frequency voltage period $T = 1/2\pi f = 0.16\,\mu$s. The B structure (the inset below) exhibits the stepped rise G_{ac} near the voltages $V = 1.65$ and 2.2 V, at which there is evidently a sharp stepped rise of the stationary current (Figure 2, the curve *2*). The amplitude of the capacitance reactive component ωC increases with the voltage more monotonously, but both the structures also exhibit a faster increase in ωC within the region of the steps of the curves $G_{ac}(V)$, on the curves $\omega C(V)$. When the amplitude of active conductance is equal to the amplitude of capacitance conductance $G_{ac} = \omega C$, then a sharp drop of the measured capacitance starts. The capacitance passes over zero ($C = 0$) at the voltage $V_0 = 2.87$ and 2.81 V in the A and B structures, respectively. With further increase in the voltage $V > V_0$, the capacitance being measured becomes negative ($C < 0$) and quickly increases in an absolute value.

The correlation between a behavior nature of the measured capacitance and the transient and the direct current observed in increase in the forward voltage indicates the following. With forward bias of the nanostructure, the barrier capacitance of the p–n-junction is supplemented with the capacitance C_{hop} that is related to the in-voltage period change of the concentration of the main carriers that are tunneled into the quantum well through the triangular potential walls, and to in-wall accumulation of the main carriers occupying the ionized localized states. Similar to the diffusion capacitance of a homojunction caused by diffusion of the minority carriers, the capacitance C_{hop} can be referred to as a diffusion capacitance caused by jump diffusion of the main carriers.

3.3. Inductive dynamic response and drop of efficiency of emission from the quantum well with increase in direct voltage

Figure 4, *a, b* shows the dependences of the direct current's differential conductance on the forward voltage $G_{dc}(V) = dI/dV$ for the A and B structures (the curves *1*), which are obtained by differentiating the I–V-curves, and on the forward bias of the p–n-junction $G_{dc}(V_j) = dI/dV_j$, $V_j = V - Ir_s$ (the curves *2*), which is determined taking into account the voltage drop on the serial resistance of the structure r_s, that was estimated from a slope of the I–V-characteristics at the rated current $I = 20$ mA to be $r_s = 8.2$ and 14.5 Ω in the A and B structures, respectively. Figure 4, *a, b* also shows the dependences of the small-signal amplitudes of the active G_{ac} (the curves *3*) and the reactive (the capacitance ωC at $V < V_0$ (the curves *4*) and the inductive $1/\omega L$ at $V > V_0$ (the curves *5*)) components of the small-signal admittance at the frequency of $f = 1$ MHz, on the forward voltage. Here, $C > 0$ — the measured capacitance and L — inductance, whose reactive conductance is equivalent to the conductance of the negative capacitance: $1/\omega L = \omega C$ at $C < 0$. Figure 4, *a, b* also shows the dependences of quantum efficiency of emission η on the forward voltage (the curves *6*) for the A and B structures.

As can be seen on Figure 4 (the curves *1* and *3*), at the threshold voltage $V_{th} = 2.2$ V, the amplitude of active conductance at the frequency of $f = 1$ MHz exceeds the direct current's conductance: $G_{ac} > G_{dc}$, but at $V > V_{th}$ already near the threshold voltage, at $V = 2.4$ V in the A structure and $V = 2.54$ V in the B structure, G_{ac} and G_{dc} become equal to $G_{dc} = G_{ac}$, and with further increase in the voltage G_{ac} becomes less than G_{dc} in both the structures $G_{ac} < G_{dc}$. In both the structures, the amplitude of the inductive conductance increases within the voltage interval $V = 2.8$–3.8 V by more than two orders, wherein in the B structure it increases with the voltage faster then in the A structure. Within the region of the high voltages, both the inductive and the active components of the high-frequency

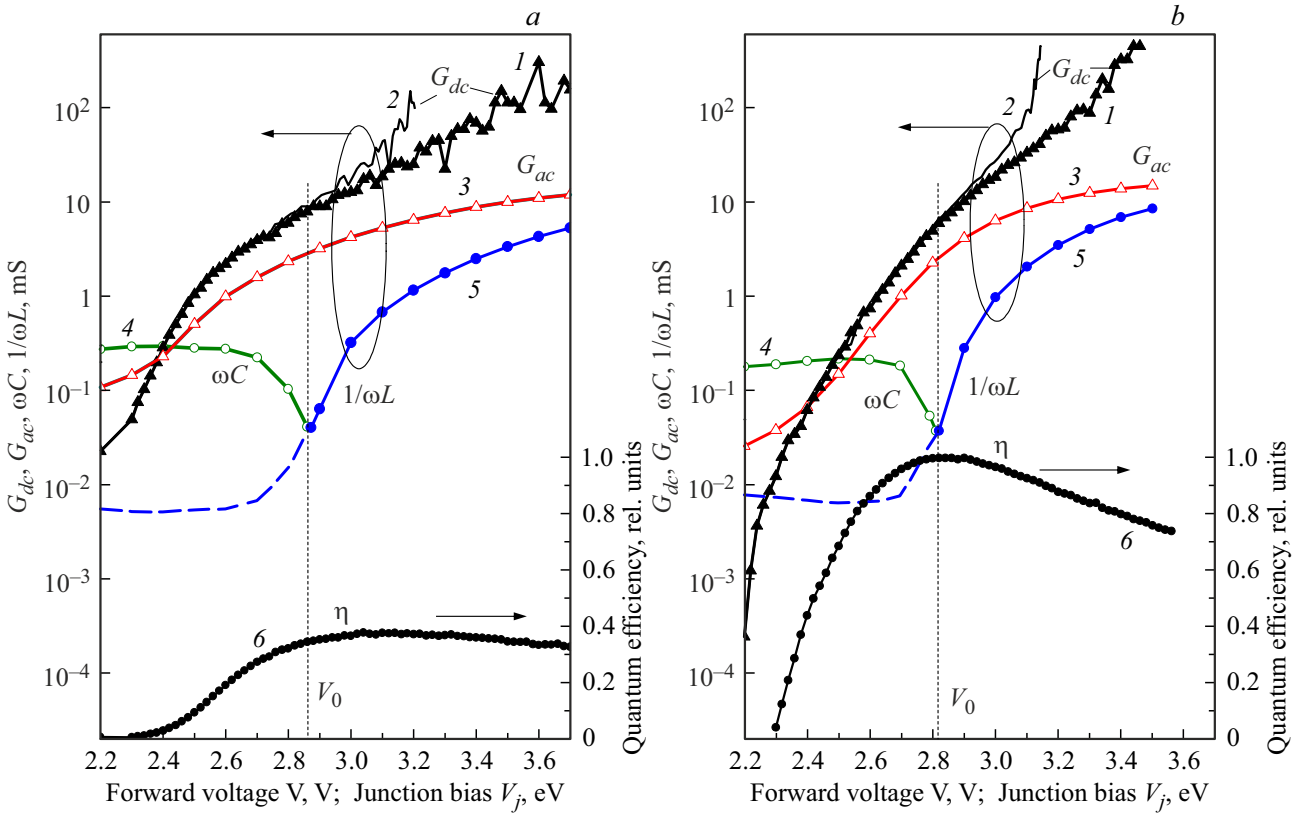

Figure 4. Dependences of differential conductance at the direct current G_{dc} on the forward voltage V (*1*) and the forward bias of the $p-n$-junction V_j (*2*), dependences of the small-signal amplitude of the active G_{ac} (*3*) and the reactive (the conductance ωC (*3*) and the inductive $1/\omega L$ (*5*)) components of small-signal admittance at the frequency of 1 MHz and the dependences of quantum efficiency η (*6*) on the forward voltage V for the A (*a*) and B (*b*) structures. The dashed lines mark the voltages $V_0 = 2.87$ (*a*) and 2.81 V (*b*), at which the zero capacitance $C = 0$ is observed.

admittance are still below the conductance G_{dc} by more than one order.

With increase in the forward voltage, the free carriers screening the external field for the short Maxwell time (at $N_a \approx 2 \cdot 10^{17}\,\mathrm{cm}^{-3}$ τ_M, it is about several picoseconds) end up at the SCR boundaries and create in the SCR a homogeneous external field directed opposite to the built-in field of the barrier. At the same time, the width of the SCR barrier quickly decreases in accordance with the value and the direction of the changed bias. Then, a slow stage of the process of screening of the external field starts due to recharging of the deep centers, which causes slow SCR widening, decrease in the SCR field strength and concentration of the external field in the quantum well walls.

With the small-signal measurements, the full voltage $V_{ac}(t) = V + v(t)$, where $v(t) = V_1 \exp(j\omega t)$, and the full tunnel current $I_{ac}(t) = I + I_1 \exp(j\omega t)$, where V and $I = I_s \exp(qV_0/nkT)$ — direct voltage and constant current density, V_1 and I_1 — the small-signal amplitudes of alternating voltage and current density, respectively. At $V_1 \ll V_0$, the small-signal variable component of the hole concentration: $\tilde{p}(x,t) = (qV_1/nkT)p_0 \exp(jwt)$, where p_0 — the stationary concentration of the holes at the border with the quantum well.

With the constant bias, the set distribution of the concentration of the tunneling holes in the well wall is determined by an equality of the rate of their jump diffusion into the wall and the rate of recombination in the wall, which is determined by the lifetime and the component p/τ. With the small-signal measurements, the rate of recombination during the voltage period varies in phase with the voltage $v(t)$ at $(\tilde{p}/\tau)j\omega\tau$ as a result of variation of the hole concentration and in antiphase with the voltage $v(t)$ at $-(\tilde{o}/\tau)(j/\omega\tau)$ as a result of variation of the lifetime. In doing so, the continuity equation [30] for the variable hole concentration in the well wall takes the form

$$D\frac{d^2\tilde{p}}{dx^2} - \frac{\tilde{p}}{\tau}\left(1 + j\left(\omega\tau - \frac{1}{\omega\tau}\right)\right) = 0.$$

The obtained equation is identical to the equation of diffusion of the free carriers through the potential barrier and recombination thereof in SCR in case $\tau = \mathrm{const}$, if the lifetime of the tunneling carriers is expressed as follows

$$\tau^* = \frac{\tau}{1 + j\left(\omega\tau - \frac{1}{\omega\tau}\right)}.$$

The frequency of jumps of the charge carriers between the occupied initial center i and the finite empty center j,

as separated by the distance R_{ij}, is [6]:

$$\nu(R_{ij}) = \nu_0 \exp(-2\gamma R_{ij}), \quad (1)$$

where $\nu_0 \approx 10^{12}\,\mathrm{c}^{-1}$ — the frequency of attempts, $\gamma = 1/a$ — the degree of overlapping of the wave functions, a — the Bohr radius. Taking into account that $I_s = qDp_0/L$, $L = R_{ij}$ and the effective microscopic diffusion constant $D = R_{ij}^2 \cdot \nu_{hop}(E_t)$, $I_s = qR_{ij}p_0/\tau$, and by respectively inserting, we obtain for the density of alternating current I_1:

$$I_1 = \frac{qV_1}{nkT} \cdot \frac{qR_{ij}p_0}{\tau}\left[1 + j\left(\omega\tau - \frac{1}{j\omega\tau}\right)\right].$$

By introducing the designations, $G_{\mathrm{ac}} = qI_s/nkT$, $C_{hop} = qI_s\tau/nkT$ and $L_{hop} = nkT/qI_s\tau$, for alternating-current's admittance we obtain:

$$Y = \frac{I_1}{V_1} = G_{ac} + j\left(\omega C_{hop} - \frac{1}{\omega L_{hop}}\right).$$

At the frequency $f_0 = 1\,\mathrm{MHz}$ and $\omega_0 = 2\pi f_0$, with the bias of V_0, $\omega_0 C_{hop} = 1/\omega_0 L_{hop}$, $\omega_0 = 1\sqrt{L_{hop}C_{hop}}$, and the small-signal conductance has only the active component G_{ac}. The dependences of the inductive component of admittance at the voltages $V < V_0$ for the A and B structures, as dashed on Figure 4, *a, b*, are obtained taking into account the following. At the voltages $V < V_0$, the SCR width change as a result of recharging of the deep centers poorly contributes to the measured capacitance in comparison with contribution of the recombination current, and the changes of the capacitance and inductance values at the fixed voltage V in relation to their value at V_0 are $\Delta\omega C_{hop} = \Delta 1/\omega L_{hop}$ and $\lg(1/\omega L_{hop}) = -2\lg(\omega C_{hop})$.

At $V = V_0$ $G_{ac} < G_{dc}$ (Figure 4, *a, b*, the curves *3* and *1*), since the stationary distribution of the hole concentration is still not set. The process of occupying the empty finite states at the tunnel transport level E_{tp} is not exponential and it slows as the empty finite states of the ionized local centers are occupied and the number of the empty states at the level E_{tp} is quickly reduced. The rate of jump diffusion is limited by jumps from the occupied states into the unoccupied states. As per (1), the jump time increases with increase in the distance between the occupied and empty local centers R_{ij} as $t(R_{ij}) = (1/\nu_0)\exp(2\gamma R_{ij})$ and in a stationary mode, a process of setting of the stationary current at the inter-center distance R_{ij} logarithmically depends on the time $R_{ij} = (1/2\gamma)\ln(\nu_0 t)$.

In the set mode, the concentration of the injected main carriers (holes) poorly changes along the tunneling length R_{ij} in the well wall. At the same time, the flowrates of the holes radiatively recombining in the well and nonradiatively in the well wall are determined by a ratio of the carrier lifetime due to nonradiative recombination in the well wall and the lifetime due to radiative recombination in the quantum well. $\tau_{n/\mathrm{rad}}/\tau_{\mathrm{rad}}$, and the quantum efficiency of radiative recombination is

$$\eta = \frac{\tau_{n/\mathrm{rad}}}{\tau_{\mathrm{rad}} + \tau_{n/\mathrm{rad}}}.$$

Since the amplitude of the inductive reactive conductance means a value of the tunnel-recombination flowrate of the injected carriers from the quantum well, then there is evidently a correlation of the dependences of the inductive component of conductance $1/\omega L$ and quantum efficiency η on the voltage (Figure 4, *a, b*, the curves *5* and *6*).

Near the threshold voltage, the main current flowing near the hole and electron tunnel transport levels E_{tp} and E_{tn} is the tunnel-recombination current in the well wall in the *p*-barrier. Only a small number of the thermally excited carriers are injected into the quantum well and the quantum efficiency is low. With increase in the voltage, the number of the carriers injected through the effective barrier quickly increases. In accordance with the neutrality condition, the same number of electrons is injected through the *n*-barrier in a tunnel way. Since the carriers radiatively recombine in pairs in the quantum well, with increase in the voltage the emission intensity exponentially rises as $\exp(qV/kT)$ due to exponential reduction of τ_{rad} with increase in the concentration of the injected holes, while the fraction of the tunnel-recombination current into the well wall decreases. As a result, within the voltage interval $V = 2.2{-}2.5\,\mathrm{V}$ the efficiency quickly increases, while the inductive reactive conductance $1/\omega L$ weakly decreases. Within the interval $V_0 > V > 2.5\,\mathrm{V}$, reduction of the tunnel transparency of the well walls and increase in the voltage drop in the walls (due to recharging of the deep centers) result in exponential increase in the pace of nonradiative recombination. It is caused by increase in the number of the states of the Urbach tails between the transport levels E_{tp} and E_{tp} (the recombination centers) increase in the depth of electron penetration in the SCR of the *p*-barrier. As a result, the efficiency increase with voltage slows, while the inductive conductance $1/\omega L$ starts rising. With further increase in the voltage $V > V_0$, the higher and higher fraction of the voltage increment drops at the well walls, thereby resulting in fast rise of the inductive conductance and in the efficiency drop.

In the A structure, the high density of states of the Urbach tails provides for high tunnel transparency of the *p*-barrier and a high rate of nonradiative recombination, and increase in the injection levels with increase in the voltage results only in decelerated and slight rise of the emission efficiency. In the B structure, the energy spectrum is dominated by the Gaussian impurity bands of the color centers, and increase in the density thereof at the level E_{tp} with increase in the voltage provides for strong increase in the efficiency with increase in the voltage. In both the structures, the zero capacitance and a start of inductive rise of the tunnel current and the efficiency drop are observed near the voltage of 2.8 V, which corresponds to the level E_{tp}'s intersection of the Gaussian impurity band of the BL-centers that are responsible for blue photoluminescence in the *p*-GaN layers. The low efficiency in the A structure corresponds to the low density of the BL- and UVL-centers in the lightly doped *p*-GaN layers [14].

4. Conclusion

The results of measurements of the transient currents at the surge of forward voltage and small-signal high-frequency conductance at constant forward bias of the light-emitting $p-n$-structures with the InGaN/GaN quantum wells have been analyzed to show a governing influence of the strong built-in field in the potential walls of the quantum well and its reduction at direct biases on confinement of the charge carriers in the quantum well. The strong field is created by the ionized deep centers to provide for tunnel injection into the quantum well through the effective barrier. During screening of the external field in forward bias, the fast reduction of the effective barrier height and its narrowing for the Maxwell time are followed by screening of the external potential by the bulk charge of the deep centers, which is accompanied by slow SCR extension and reduction of the field strength in the well walls due to recharging of the deep centers. The recharging of the deep centers results in reduction of the tunnel transparency and increase in the tunnel resistance of the wall and the voltage drop in the wall, which is accompanied by exponential reduction of the nonradiative lifetime in the wall and drop of the quantum efficiency of emission from the quantum well. Capturing of the main carriers and respective reduction of the bulk charge in the wall dominate at small biases and are manifested as an exponentially slowing decay of the transient current at the surge of forward bias and capacitance dynamic response. The nonradiative recombination of the captured carriers dominates at high biases and is manifested as slow rise of the transient current and the inductive dynamic response.

Conflict of interest

The authors declare that they have no conflict of interest.

References

[1] C.H. Qiu, C. Hoggatt, W. Melton, M.W. Leksono, J.I. Pankove. Appl. Phys. Lett. **66**, *20*, 2712 (1995).
[2] O. Ambacher, W. Reiger, P. Ansmann, H. Angerer, T.D. Moustakas, M. Stutzmann. Solid Stat. Commun. **97**, *5*, 365 (1996).
[3] P. Perlin, M. Osinski, P.G. Eliseev, V.A. Smagley, J. Mu, M. Banas, P. Sartori. Appl. Phys. Lett. **69**, *12*, 1680 (1996).
[4] C. Gourdon, P. Lavallard. Phys. Status Solidi B **153**, *2*, 641 (1989).
[5] E.L. Ivchenko, A.N. Reznitsky. Phil. Mag. B **65**, *4*, 733 (1992).
[6] D. Monroe. Phys. Rev. Lett. **54**, *2*, 146 (1985).
[7] L. Esaki. Phys. Rev. **109**, *2*, 603 (1958).
[8] In: Tunneling phenomena in solids / Ed. E. Burstain, S. Lundqvist / Plenium Press, N.Y. (1969). Ch. 5.
[9] A.G. Chynoweth, W.L. Feldmann, R.A. Logan. Phys. Rev. **121**, *3*, 684 (1961).
[10] N. Holonyak. J. Appl. Phys. **32**, *10*, 130 (1961).
[11] N. Holonyak, Jr., D.L. Keune, R.D. Burnham, C.B. Duke. Phys. Rev. Lett. **24**, *11*, 580 (1970).
[12] S.F. Chichibu, Y. Kawakami, T. Sota. In Introduction to Nitride Semiconductor Blue Lasers and Light Emitting Diodes / Ed. S. Naramura, S.F. Chichibu. Taylor & Francis, L., N.Y. (2000). Ch. 5.
[13] M.A. Reshchikov, H.J. Morkoç. J. Appl. Phys. **97**, 061301 (2005).
[14] S.F. Chichibu, A. Uedono, K. Kojima, H. Ikeda, K. Fujito, S. Takashima, M. Edo, K. Ueno, S. Ishibashi. J. Appl. Phys. **123**, 161413 (2018).
[15] N.I. Bochkareva, I.A. Sheremet, Yu.G. Shreter. FTP **50**, *10*, 1387 (2016). (in Russian).
[16] C. Ostermaier, P. Lagger, G. Prechtl, A. Grill, T. Grasser, D. Pogany. Appl. Phys. Lett. **110**, 173502 (2017).
[17] N. Roccato, F. Piva1, C. Santi, M. Buffolo, C. Haller, J.-F. Carlin, N. Grandjean, M. Vallone, A. Tibaldi, F. Bertazzi, M. Goano, G. Verzellesi, G. Meneghesso, E. Zanoni, M. Meneghini. J. Phys. D **54**, 425105 (2021).
[18] A.M. Ionescu, H. Riel. Nature **479**, *7373*, 329 (2011).
[19] D. Sarkar, X. Xie1, W. Liu, W. Cao, J. Kang, Y. Gong, S. Kraemer, P.M. Ajayan, K. Banerjee. Nature **526**, *7571*, 91 (2015).
[20] T. Ohno, Yu. Oyama. Sci. Technol. Adv. Mater. **13**, *1*, 013002 (2012).
[21] N. Moulin, M. Amara, F. Mandorio, M. Lemiti. J. Appl. Phys. **126**, 033105 (2019).
[22] A. Schenk, S. Sant. J. Appl. Phys. **128**, 014502 (2020).
[23] E.-M. Bourim, J.I. Han. Electron. Mater. Lett. **12**, *1*, 67 (2016).
[24] N.I. Bochkareva, Yu.G. Shreter. FTT **64**, *3*, 371 (2022). (in Russian).
[25] N.I. Bochkareva, Yu.G. Shreter. FTT **65**, *1*, 138 (2023). (in Russian).
[26] N.I. Bochkareva, Yu.G. Shreter. ZhTF **94**, *8*, 1158 (2023). (in Russian).
[27] S. Nakamura, M. Senoh, N. Iwasa, S. Nagahama, T. Yamada, T. Mukai. Jpn. J. Appl. Phys. Part 2 **34**, L1332 (1995).
[28] Y.T. Rebane, N.I. Bochkareva, V.E. Bougrov, D.V. Tarkhin, Y.G. Shreter, E.A. Girnov, S.I. Stepanov, W.N. Wang, P.T. Chang, P.J. Wang. Proc. of SPIE **4996**, 113 (2003).
[29] L.V. Keldysh. ZhTF **33**, *4*, 994 (1957); **34**, *4*, 962 (1958). (in Russian).
[30] G.E. Pikus. Osnovy teorii poluprovodnikovykh priborov. Nauka, M., (1965). 448 p. (in Russian).

Translated by M.Shevelev